(1970); W. M. McClain, *J. Chem. Phys.*, **55**, 2789 (1971).
4. D. M. Friedrich, *J. Chem. Ed.*, **59**, 572 (1982).
5. D. Lee, *Bull. Korean Chem., Soc.*, **8**, 338 (1987).
6. T. J. Spiro and T. C. Strekas, *Proc. Nat. Acad. Sci. USA*, **69**, 2622 (1972).
7. M. Goeppert Mayer, *Ann. Phys.*, **9**, 273 (1931).
8. D. Lee and A. C. Albrecht, *Adv. Infrared and Raman Spectroscopy*, **12**, 179 (1985).
9. R. Pariser, *J. Chem. Phys.*, **24**, 250 (1956).
10. P. R. Callis, T. W. Scott and A. C. Albrecht, *J. Chem. Phys.*, **78**, 16 (1983).
11. J. Del Bene and H. H. Jaffe, *J. Chem. Phys.*, **48**, 1807 (1968); J. Del Bene and H. H. Jaffe, *J. Chem. Phys.*, **49**, 1221 (1968).
12. G. Hohlneicher and B. Dick, *J. Chem. Phys.*, **70**, 5427 (1979); F. T. Marchese, C. J. Seliskar and H. H. Jaffe, *J. Chem. Phys.*, **72**, 4194 (1980).
13. J. Tang and A. C. Albrecht, *Raman Spectroscopy*, ed. H. Szymanski (Plenum, New York, 1970).

Species Selective Spectroelectrochemistry Employing Derivative Absorbance Signals

Chaojiong Zhang† and Su-Moon Park*

Department of Chemistry, University of New Mexico, Albuquerque, NM 87131, U.S.A.

Received March 6, 1989

Species selective spectroelectrochemistry (SSSE) is described by relating the derivative absorbance (dA/dt) signals with electrochemical currents for conventional transient electrochemical experiments. Expressions relating the currents with the dA/dt signals were obtained. From these expressions, physical constants such as diffusion coefficients and molar absorptivities of electrogenerated species can be determined. By obtaining both derivative absorbance and current signals concurrently and comparing them, one can perform the SSSE experiments. The utility of the SSSE in sorting out electrochemical information is demonstrated.

Introduction

Although the concept of the species selective electrochemistry (SSSE) has been recognized in the earlier literature[1-5] on spectroelectrochemical techniques, the general comparison of absorbance and current signals has not been made explicitly so that the SSSE may be implemented in conventional transient electrochemical experiments. Bancroft *et al.*[6] reported a spectroelectrochemical experiment equivalent to cyclic voltammetry by obtaining the dA/dE signal, where A and E represent the absorbance and the potential, respectively. The dA/dE signal has the identical shape to the cyclic voltammetric current, but the two showed different scan rate dependencies. These authors also demonstrated that the double layer charging current can be eliminated by running chronoabsorptometry instead of chronocoulometry,[7] if the electrogenerated species absorbs photons.

We have recently developed near normal incidence reflectance spectroelectrochemical (NNIRS) techniques using a bifurcated optical fiber probe.[8] This system is a modified version of the experimental arrangement reported by McCreery *et al.*[9] such that the angle of the probing beam would be nearly normal to the reflective working electrode. The NNIRS technique offers simplicity at the expense of sensitivity, when compared to the system described by McCreery *et al.*[9] Its fully supported microcomputer controlled data acquisition system allows easy treatment of the data. Due to the fast and undistorted electrochemical responses owing to its favorable cell geometries, this system is suitable for making nonequilibrium spectroelectrochemical measurements. Its utility for studying electrochemically generated intermediates, both solution and surface bound species such as oxide and polymer films formed on electrode surfaces, has been demonstrated.[10-13]

In our current communication, we describe equations relating dA/dt signals with currents for transient electrochemical experiments, and discuss the concept of the SSSE from the results obtained using the NNIRS system. Thus, the concurrent measurement of optical and electrochemical signals allows us to carry out the SSSE for traditional transient electrochemical experiments such as cyclic voltammetry, chronoamperometry/chronocoulometry, and chronopotentiometry. The SSSE can be a powerful tool for studying complex electrochemical reactions.

Experimental

The chemicals were all ACS reagent grade or better, and were used as received without further purification. Doubly distilled, deionized water was used for preparing solutions. Solutions were deaerated by bubbling with nitrogen gas, and the nitrogen atmosphere was maintained throughout the ex-

† Department od Chemical Engineering, Texas A & M University, College Station, TX 77843, U.S.A. *Department of Chemistry, Pohang Institute of Science and Technology, Pohang 790-600, Korea

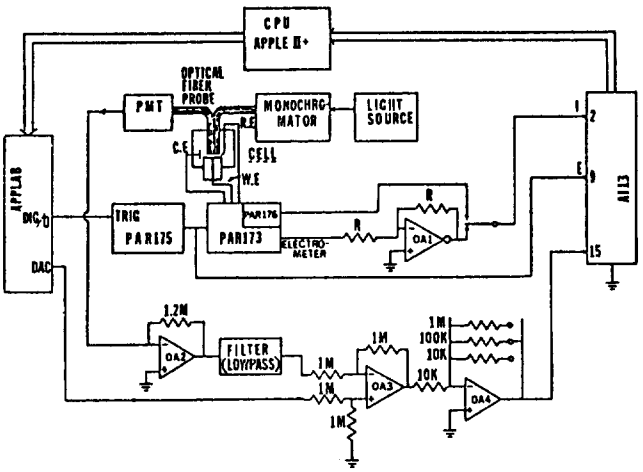

Figure 1. A block diagram for interfacing the NNIRS system with an APPLE II + Computer. See the text for details.

periment.

The electrochemical cell used in this study had two compartments: working and counter electrode compartments.[14] Both working and reference electrodes were housed in the working compartment, while a platinum wire spiral electrode was separated from them with a fine glass frit to prevent any oxidation or reduction products from diffusing back to the working compartment. The working electrode (Sargent Welch S-30101-20) was a platinum disk sealed flush to the glass surface and having a diameter of 0.65 cm. This electrode was polished to a mirror finish down to 0.1μ using alumina powder (Fischer) and then cleaned in a hot 3 M HNO_3 solution followed by rinsing in an ultrasonic vibrator to remove small alumina particles. An Ag/AgCl, satd. KCl electrode was used as a reference electrode unless otherwise mentioned.

The bifurcated fiber optical beam probe was located 0.1-1 cm above the working electrode. The bifurcated fiber optics cable was custom made by Dolan-Jenner (Woburn, MA) with optical grade quartz fibers. The merged side of the probe had 3.8 mm (diameter) of the fiber bundle. The illumination area through the fiber bundle was smaller than that of the electrode; thus the linear diffusion condition would be maintained in the optically probed area. The spectral region of this fiber was about 220-800 nm. The detector used for reflected light from the electrode surface was a Hammamatsu R955 photomultiplier tube, which has a practically flat response in the spectral region of 195-900 nm. The light source was a GCA/McPherson model 701-50, which had both deuterium and tungsten lamps.

The data acquisition was achieved practically in the same manner as described in our earlier communication[8]; a slight modification was made for fast simultaneous recording of both electrochemical and spectroscopic signals. When the time dependencies of currents, absorbances at fixed wavelengths, and/or potentials were studied, the interface shown in Figure 1 was used. As can be seen in Figure 1, the system consists of an APPLE II + microcomputer system, a Princeton Applied Research (PAR) 175 function generator, and a PAR 173 potentiosat/galvanostat with a PAR 176 current-voltage converter. Linking these instruments and the computer are two plug-in boards, *i.e.*, and APPLAB card (Interactive Microware, Inc., State College, PA) and an AI13 fast analog-to-digital converter (ADC) card (Bala Cynwyd, PA). The AI13 board has a 13-bit 7919 successive approximation ADC (Intersil) with 16-channel inputs. This ADC has a conversion time of 20μs with its sampling aperture of 125 ns.

The general sequence of experimental procedure is as follows: First the spectrum of an electrogenerated species is obtained as previously described,[8] from which a proper wavelength is chosen. Then, the reflectance intensity at that particular wavelength is recorded without an electrochemical perturbation. This intensity is later used as a reference through the digital-to-analog converter (DAC) on the APPLAB board. Finally, when the experiment begins, the signal obtained from the PMT is now compared by a differential amplifier (OA3, Figure 1), whose output, *i.e.*, differential reflectance (ΔR) is recorded as a function of time through a channel of the fast ADC on the AI13 board. The differential signal ΔR can be amplified to provide higher sensitivities. When the experiment begins, the PAR 175 function generator is triggered by a pulse from the digital output coming from the VIA (versatile interface adaptor) on the APPLAB board to generate a preprogrammed potential pulse or sweep. While the optical signal is being recorded, the current output from the PAR 176 current/voltage converter or the voltage output from the electrometer on the PAR 173 galvanostat/potentiostat is digitized using one of the other channels of the AI13. We chose to take advantage of functions built into the PAR 175 universal programmer, because the APPLE II + computer proved too slow for generating the voltage ramp through the DAC and the subsequent data acquisition. Thus, the applied potentials and their resultant currents from the electrochemical cell were digitized using two channels on the AI13 board. The main program incorporating all these operations was written in BASIC, but the data acquisition and control subroutines were written in 6502 assembly language.

Since the signal (ΔR) read by the AI13 at the output of OA3 (Figure 1) is the differential reflectance, the absorbance at any time is calculated from the equation,

$$A(t) = \log\left[\frac{R - \Delta R(t)}{R}\right] \tag{1}$$

where R (reference reflectance) is independent of time. The chronocoulometry was obtained by numerically integrating the chronoamperometric signals using the computer. The dA/dt signals were obtained by differentiating absorbance signals.

Results and Discussion

Equations Relating Absorbance Signals with Electrochemical Currents. Before discussing the results, we first present a brief theoretical consideration for relating electrochemical signals with absorbance. The absorbance for an electrochemically generated species *Red* according to an electrochemical reaction,

$$O_x + ne^- \rightleftharpoons Red \tag{2}$$

is obtained from the equation[15],

$$A = \varepsilon_R \int_0^\infty C_R(x, t)\, dx \tag{3}$$

where ε_R is the molar absorptivity of *Red* and C_R is the concentration of electrogenerated *Red* at a distance x from the electrode surface at an electrolysis time of t. Obtaining complete expressions for the absorbance according to eq. (3) under various electrolysis conditions is difficult; $C_R(x,t)$ must be known under the boundary conditions where experiments are run. However, a simple relation,

$$\frac{dA}{dt}=\frac{2000 i \varepsilon_R}{nFS} \tag{4}$$

is obtained by realizing a simple equation that relates absorbance A with charge Q.[14] Here S is the electrode area and the factor 2 comes in due to the fact that the probing beam passes through the absorbing medium twice in NNIRS experiments. From eq.(4), we obtain almost any dA/dt expressions corresponding electrochemical current; for example, we obtain the diffusion limited equation,

$$\left[\frac{dA}{dt}\right]_d=2000\varepsilon_R C_o^*\left[\frac{D_o}{\pi t}\right]^{1/2} \tag{5}$$

by using the Cottrell equation for i_d in eq.(4). Integration of eq.(5) leads to the familiar expression for chronoabsorptometry,[15]

$$A(t)=4000\varepsilon_R C_o^*\left[\frac{D_o\cdot t}{\pi}\right]^{1/2} \tag{6}$$

For cyclic voltammetry, we obtain

$$\left[\frac{dA}{dt}\right]_p=5.58\times10^3\varepsilon_R n^{1/2} D_o^{1/2} v^{1/2} C_o^* \tag{7}$$

from the Randles-Sevcik equation for reversible electron transfer. Here v is the scan rate in volts/s and other symbols follow their usual meanings. Note that any expressions can be derived straightforwardly using eq.(4) as long as current expressions are known. Notice also that no assumptions have been made for eq.(4) concerning the reversibility. Current expressions have been derived for most experimental conditions.[15]

The dA/dE *vs.* E (potential) plot was first described by Bancroft *et al.*,[6,7] and called derivative cyclic voltabsorptometry (DCVA). The expression for dA/dE has the form,[6]

$$\left[\frac{dA}{dE}\right]_p=0.881\cdot\varepsilon_R\cdot D_o^{1/2}\cdot C_o^*\cdot v^{-\frac{1}{2}} \tag{8}$$

which has a different scan rate dependency from eq.(7) as well as from cyclic voltammetry (CV). The Randles-Sevcik equation for CV,[15]

$$i_p=2.69\times10^5\cdot n^{3/2}\cdot S\cdot D_o^{3/2}\cdot C_o^*\cdot v^{1/2} \tag{9}$$

and eq.(7) can be directly compared in their shape, whereas eq.(8) may provide some complimentary information. Assuming that there is no significant nonfaradaic contribution to a cyclic voltammogram, CV and DCVA should be identical in their shapes with their relative signal magnitudes normalized. Thus, the division of eq.(7) by eq.(9), followed by slight rearrangements, results in an expression,

$$\varepsilon_R=48.2\cdot n\cdot S\frac{(dA/dt)_p}{i_p} \tag{10}$$

which allows us to determine ε_R with only S (electrode area) known. If the two do not match, however, it is an indication that the electrochemistry or chemistry involved must have some other complications and therefore must be sorted out.

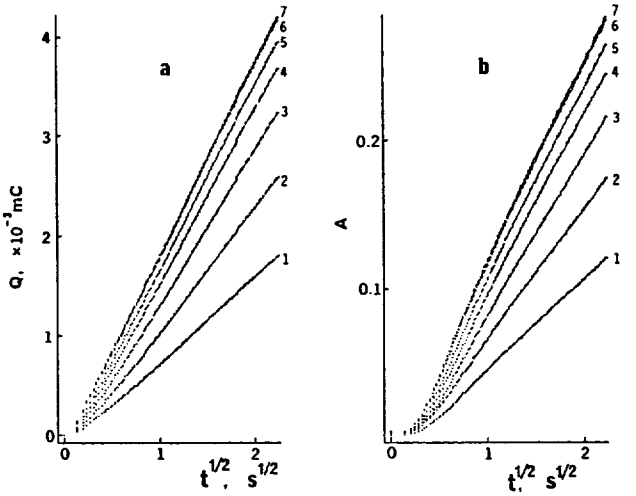

Figure 2. Anson plots obtained from the potentiostatic oxidation of the ferrocyanide ion (20.0 mM) in 0.50 M NaCl and 0.1 M phosphate buffer (pH = 6.60). Potentials applied were: 1) 0.250, 2) 0.270, 3) 0.290, 4) 0.310, 5) 0.330, 6) 0.350, and 7) 0.390 V vs. Ag/AgCl electrode from the initial potential of 0.090 V. a) From chronocoulograms recorded. b) From chronoabsorptograms.

The concept of the SSSE can also be applied to chronopotentiometric experiments provided that reactants or products of an electrochemical reaction absorb photons. Since the current applied is constant or programmed in chronopotentiometric experiments, its chronoabsorptogram should assume a linear or an integrated form of the programmed current. The dA/dt curve should then represent the current efficiency, which may be related to the change in potentials in a chronopotentiogram. This information can be used for correcting transition times or related to certain chemical reactions.

Chronocoulometry / Chronoabsorptometry. As a control, we ran potential step experiments using the ferricyanide/ferrocyanide redox pair, which has been studied thoroughly by Blount *et al.*[7,16] Chronocoulograms and chronoabsorptograms were obtained by stepping potentials to a series of different values from the initial potential of 0.09 V (not shown). The corresponding Anson plots[14,17] are shown in Figures 2(a) and 2(b). Chronoabsorptograms exhibit linear response regions at longer electrolysis times than the corresponding chronocoulograms, and as such, the intercepts in the $t^{1/2}$ axis are larger than those obtained from chronocoulometric experiments. Electrokinetic as well as other parameters evaluated according to procedures described in the literature[7,15,16] from these graps and Figure 3 are listed in Table 1. Note in Table 1 that the k° value obtained from chronocoulometry is apparently inflated due to the double layer charging current, which are added up to the faradaic charges in chronocoulograms and therefore the redox system shows higher apparent reversibility.

Another example is shown by the electrochemical reduction of methyl viologen dication (MV^{2+}), which is considered to undergo two reversible one electron reductions, first to the cation radical ($MV^{+\cdot}$) and then to the neutral compound (MV°).[18] The electrochemical reduction of MV^{2+} to $MV^{+\cdot}$ has been studied extensively using tin oxide transparent elec-

Table 1. Kinetic Data for Ferrocyanide Oxidation[a,b]

	Chronocoulometry	Chronoabsorptometry	Data in the Literature
$k°$, cm/s	$7.2(\pm 0.2)\times 10^{-3}$	$4.63(\pm 0.09)\times 10^{-3}$	1.4×10^{-2}[c]
			4.6×10^{-4}[d]
			4.0×10^{-4}[e]
α	0.36 ± 0.03	0.34 ± 0.03	0.43[c]
			0.328[d]
			0.323[e]
D_R, cm/s	6.8×10^{-6}	6.9×10^{-6}	6.50×10^{-6}[f]
ε_R, *l*/mole/cm	—	1.07×10^{3}	1.02×10^{3}[f]

[a] 0.10 M phosphate buffer, pH = 6.6, 20.0 mM $K_4Fe(CN)_6$. [b] Standard deviations were calculated at 95% confidence levels. [c] W. J. Bladel and G. W. Scheiffer, *J. Electroanal. Chem.*, **80**, 259 (1977). [d] By chronoabsorptometry (Ref. 16). [e] By chronocoulometry (Ref. 16). [f] N. Winograd, H. N. Blount, and T. Kuwana, *J. Phys. Chem.*, **73**, 3456 (1969).

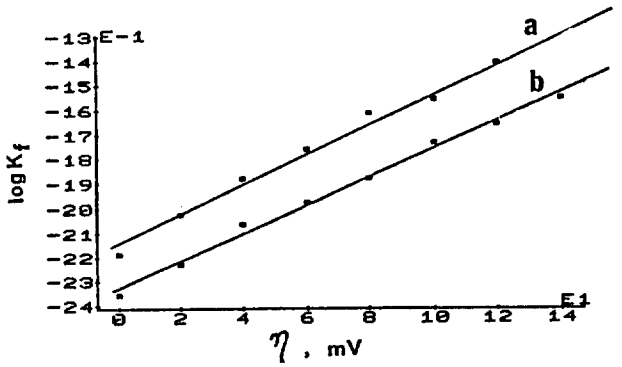

Figure 3. Log k_f *vs.* overpotential plot: a) data obtained from Figure 2(a), and b) data obtained from Figure 2(b).

trodes.[19-21]

The results obtained from potential reversal chronocoulometric and chronoabsorptometric experiments are shown in Figure 4 for the reduction of MV^{2+}. The coulometric and absorptometric results are very similar in their shapes except that the ratios of the charge (or absorbance) at 2τ to that at τ, where τ is the time at which potential is reversed, are different. This ratio is consistently around 0.414 for the coulometric charge within an experimental error, whereas it is 0.339 at 545 nm and 0.494 at 606 nm, respectively.

This result is explained by the fact that MV^{+} undergoes dimerization reaction[22,23] rather effectively with an association constant of 377 $l\cdot mole^{-1}$. Schwarz[23] assigned absorption bands at 396 and 602 nm to monomer species and those at 368 and 556 nm as dimeric species. Thus the MV^{+}, which has been regarded as a stable reduction product in most electrochemistry literature, undergoes a chemical reaction following the electron transfer. Our results also indicate that the equilibrium between the monomer and the dimer is sufficiently fast and thus, the reduction of MV^{2+} behaves as a perfectly reversible system, as indicated by the charge ratio, $Q_{2\tau}/Q_{\tau}$, of 0.414. When monitored at 606 nm (monomer), the absorbance ratio observed (0.494) shows that the MV^{2+} has a characteristics of an EC mechanism. This mechanism is supported by the absorbance ratio observed at 545 nm for the dimer, since the lower ratio (0.339) indicates that the

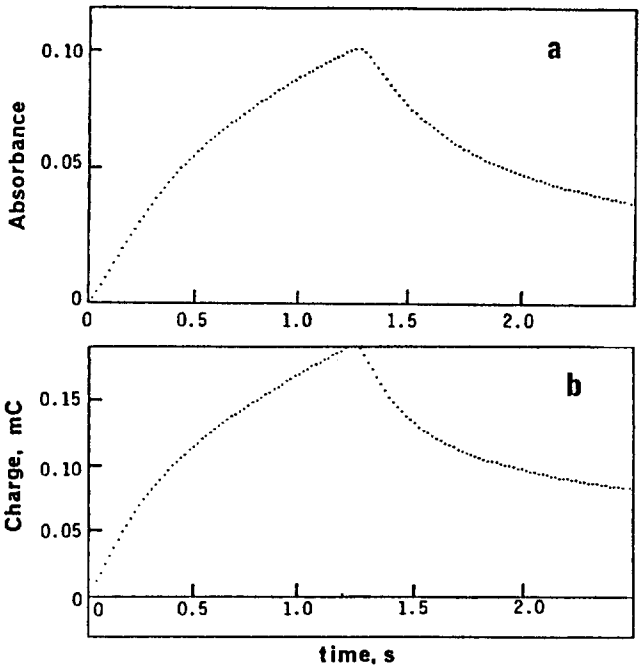

Figure 4. a) The potential reversal chronocoulogram for MV^{2+}. b) The potential reversal chronoabsorptogram for MV^{2+} simultaneously recorded at 606 nm. The solution contained 2 mM MV^{2+} and 2 M KCl. The initial potential was set at −0.10 V stepped to −0.80 V, and stepped back to −0.10 V.

dimer accumulates at the expense of the monomer. All these are the result of the competition between homogeneous and heterogeneous reactions. To our knowledge, the EC nature of this reaction has not been reported in the electrochemistry literature.

Cyclic Voltammetry / Derivative Cyclic Voltabsorptometry (DCVA). The validity of eq.(7) was demonstrated by monitoring scan rate dependencies of $(dA/dt)_p$ for the reduction of MV^{2+} at 545 and 606 nm. The results are shown in Figure 5, which indicates that the dA/dt *vs.* E plots behave as CV plots do. Manipulation of CV peak currents and $(dA/dt)_p$ signals according to eq.(10) leads to the ε_R values of 2.48×10^{3} and 2.41×10^{3} $l\cdot mole^{-1}cm^{-1}$ at 545 and 606 nm, respectively, and the D_O value of 1.9×10^{-5} cm^2/s. Since spectral bands at two wavelengths are overlapped considerably, these ε_R values should be regarded as approximate. The diffusion coefficient is somewhat higher than the one reported (0.85×10^{-5} cm^2/s) in the literature.[18]

An example for applications of DCVA to studying electrochemical processes is demonstrated by the reduction of heptyl viologen dication (HV^{2+}). The HV^{2+} is also known to undergo two step reductions eventually to HV° through HV^{+}, and the first step is regarded as reversible.[18] The reaction has received much attention due to its possible applications as an electrochromic device. The first reduction product, HV^{+}, form a blue precipitate on the electrode surface. Most spectroelectrochemical studies address first electron transfer reaction; not much has been reported on the second step reaction. This is because of the high reactivity of HV° with HV^{2+} in solution according to

$$HV^{0}+HV^{2+}\rightarrow 2HV^{+} \qquad (11)$$

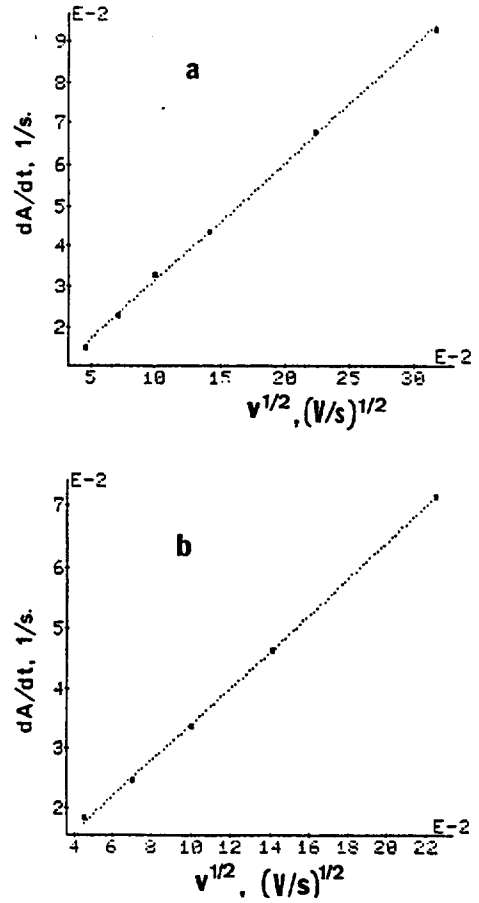

Figure 5. a) $(dA/dt)_p$ *vs.* $v^{1/2}$ (scan rate) plot for MV^{2+} reduction at 606 nm. b) $(dA/dt)_p$ *vs.* $v^{1/2}$ plot for MV^{2+} reduction at 545 nm.

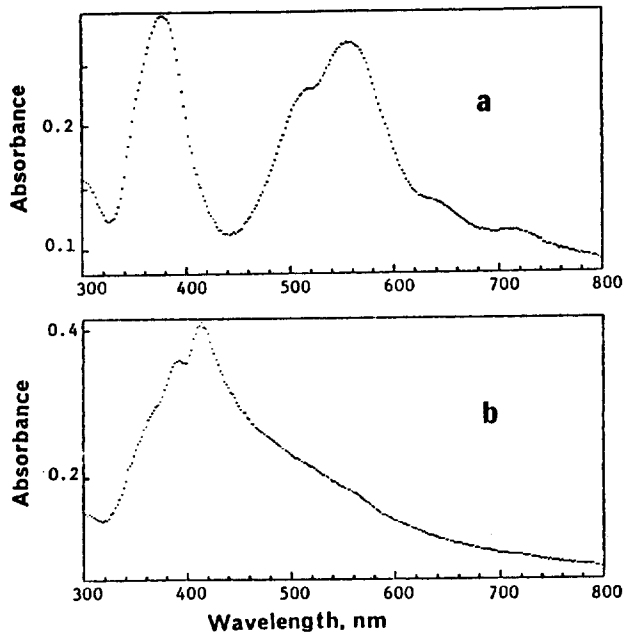

Figure 6. a) Spectrum recorded for HV^{2+} during the reduction at -0.60 V. The solution contained 4 mM HV^{2+} in 1.0M KBr solution. The spectrum was recorded in the bulk solution using the NNIRS setup. b) Spectrum recorded for HV° after complete reduction at -0.96 V. The spectrum was recorded in a thin layer cell configuration (14). Other experimental conditions were identical to those in a).

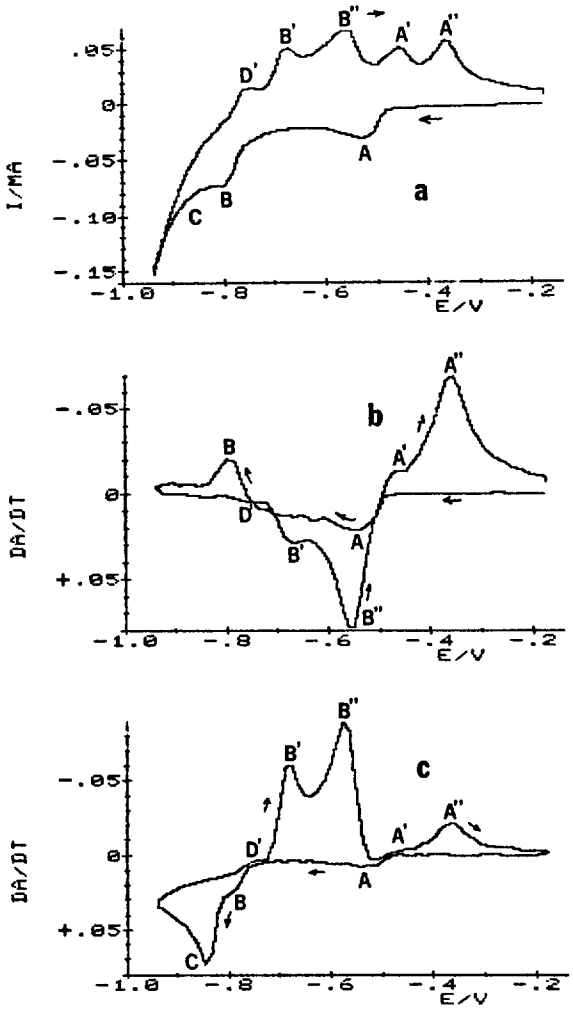

Figure 7. a) Cyclic voltammogram recorded for HV^{2+} reduction at a scan rate of 5 mV/s. The solution had 2 mM HV^{2+} in 0.30 M KBr. b) DCVA recorded at 570 nm from the same solution as in a). c) DCVA recorded at 440 nm.

As a result, the spectrum of HV° can only be recorded with exhaustive electrolysis.

Shown in Figure 6 are spectra recorded for electrogenerated HV^{+} at -0.60 V (a) and HV° at -0.96 V (b), respectively. The spectrum shown in Figure 6 (b) was recorded inside the thin layer cell[14] after exhaustive electrolysis. The spectrum of HV^{+} agrees well with those reported in the literature. From the spectra shown, we decided to monitor the radical cation at 570 nm and the neutral species at 440 nm, respectively, using DCVA. The wavelength, 440 nm, was chosen because of the trough in the spectrum of the cation radical.

Figure 7 shows CV (a), DCVA at 570 nm (b), and DCVA at 440 nm (c), all recorded at the scan rate of 5 mV/s. The CV, while simple during the cathodic scan, shows a number of current peaks during the anodic scan. The appearance of various peaks and their relative magnitudes were shown to be dependent on how long the reduced products were aged.[24] Scan rates play important roles in determining the shapes of CVs, since they also reflect the aging period.

The DCVA recorded at 570 nm monitoring the HV^{+} behavior demonstrates the HV^{+} is produced at a diffusion limited rate past the cathodic CV peak A [Figure 7(a)], reduced

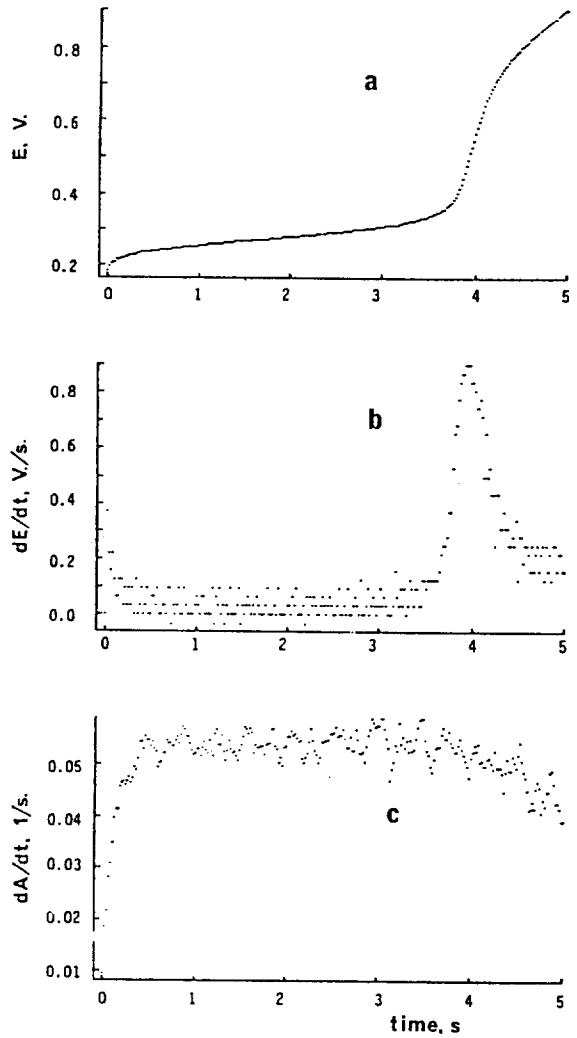

Figure 8. a) Chronopotentiogram recorded for anodic oxidation of 20.0 mM ferrocyanide in 0.50 M KCl solution. The applied current was 0.80 mA. b) *dE/dt* plot calculated from a). c) *dA/dt* plot calculated from chronoabsorptogram obtained concurrently with a).

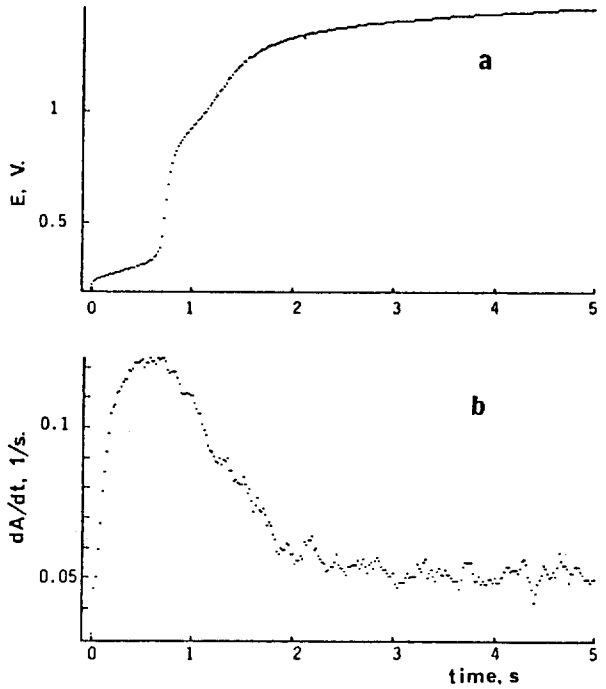

Figure 9. a) Chronopotentiogram obtained from the same solution as used in experiments for Figure 8(a). b) Accompanying *dA/dt* plot.

further to produce HV°, regenerated in three steps (peaks D', B', and B''), and finally oxidizes back to HV^{2+} in two steps (peaks A' and A''). Although high CV currents are flowing at potentials more negative than peak B, these currents originate mainly from the direct reduction of HV^{2+} to HV° [see Figure 7(b)] and hydrogen evolution [Figure 7(a)]. The DCVA shown in Figure 7(c) is largely complementary to the one in Figure 7(b). It shows that HV° is produced in two steps, one from $HV^{+\cdot}$ deposited on the surface (peak B) and the other directly from solution species HV^{2+} (peak C). Note that the latter process is diffusion controlled as *dA/dt* decreases according to the Cottrell shape until potential reversal. Again, the hydrogen evolution current, shown as a background current in Figure 7(a), is completely discriminated against. The HV° thus generated is now reoxidized back to $HV^{+\cdot}$ in three steps. We believe that the low *dA/dt* signals observed at peak positions A' and A'' [Figure 7(c)] are due to low absorbances shown by $HV^{+\cdot}$ at 440 nm. Finally, it should be pointed out that the large CV anodic peak shown by D' should be mostly from the reoxidation of absorbed hydrogen to H^+. There is a very little contribution to this peak from the oxidation of HV° to $HV^{+\cdot}$ as shown in Figure 7(c) (shoulder D'). The DCVA shown in Figure 7(c) was recorded simultaneously with the CV in Figure 7(a), but the one in Figure 7(b) was recorded in the subsequent scan.

Our observations indicate that there are at least two different forms of HV° as indicated by two different anodic *dA/dt* signals and a shoulder (D') in Figure 7(c). These two forms have the same optical properties but should differ in their phases, which affect the thermodynamics, *i.e.*, oxidation potentials. The relative magnitude of these peaks, which reflects the relative amount of each phase, varies depending upon the scan rate or the aging period. Once the different forms are generated, the corresponding phases of $HV^{+\cdot}$ are also generated, which seem to have inherited their physical properties from their precursors. When only $HV^{+\cdot}$ is produced, there is only one form of the precipitate, where a CV and corresponding DCVA have identical shapes. The importance of scan rates in determining the CV shapes has been discussed by Bruinink *et al.*[24]

Chronopotentiometry / Chronoabsorptometry. The double layer charging current has presented more problems to galvanostatic experiments than to potentiostatic methods.[15] A few approaches to either minimize or eliminate the effects exerted by the nonfaradaic component have been made.[25-27] We demonstrate here that simultaneous measurements of optical and electrochemical signals can correct for the double layer charging current. Also, this technique provides an excellent tool to selectively identify certain electrochemical process when a number of other processes take place concurrently.[28] We will examine only the first case here.

Typical results obtained from chronopotentiometric experiments are shown in Figure 8, in which a chronopotentiogram (a), the resulting *dE/dt* plot (b), and the *dA/dt* plot (c), recorded during the galvanostatic oxidation of ferrocyanide

at a current density of 0.80 mA. The *dE/dt* plot shown here provides a means of determining the transition time, τ, as was used by some investigators.[26,27] Analog electronic devices were constructed to compensate the double layer charging currents and also to determinate the position on the time axis, where the maximum value of *dE/dt* is obtained. Even though a complete compensation can be made for the double layer charging current, the time at which the maximum *dE/dt* occurs cannot be a true τ, since this occurs at the inflection point of the potential jump. The time where two current efficiency lines meet in Figure 8(c), however, represents a more accurate transition time, provided that the double layer charging current has been corrected for. This is the time at which the concentration of the electroactive species begins to be depleted and thus its current efficiency deviates from 100%. Note also in Figure 8(c) that it takes approximately 0.45s to reach the current efficiency of 100%. This time depends on parameters such as electrode areas, current densities, porosities of electrodes, and supporting electrolyte concentrations (see Figure 9).

The transition time determined from the *dE/dt* plot in Figure 8(a) is 3.95s, whereas it is 3.84s determined from the *dA/dt* plot according to the procedure described above. Both values are the ones without the correction of the double layer charging current. With the correction made to the second transition time (3.84s) by estimating nonfaradaic charge (~4.2%), the transition time becomes 3.64s. We believe that this is the transition time closer to the true value. We checked the $i \cdot t^{1/2}$ values calculated from different transition times obtained for different current densities; they show a constancy for each set of data. The $i \cdot t^{1/2}$ values obtained from *dE/dt* plots had slightly better precision (1.52 ± 0.01 mA·s$^{1/2}$) than those from *dA/dt* plots (1.40 ± 0.04 mA·s$^{1/2}$) for number of measurements. We thus conclude that the constancy of the $i \cdot t^{1/2}$ values does not necessarily provide a criterion for the accuracy of the transition time.

Although the correction for the nonfaradaic component was only about 4.2% in this case, this depends on the experimental conditions. An example for an extreme case is found in Figure 9, in which a chronopotentiogram (a) and the accompanying *dA/dt* plot (b) are shown. Here the contribution from the nonfaradaic current is estimated to be approximately 25%, due mostly to the high current density.

Conclusion

We have shown by presenting a number of examples that species selective spectroelectrochemical experiments can be performed by making simultaneous measurements of optical and electrochemical signals. Any type of transient electrochemical experiments can be combined with the spectroscopic measurements to perform the SSSE. A simple equation that relates derivative absorbance signals with electrochemical currents was given. It was demonstrated that not only various physical constants can be evaluated, but also nonfaradaic and faradaic currents that do not produce absorbing intermediates can be eliminated using the SSSE experiments. By combining a few SSSE experiments, mechanistic as well as analytical studies can be performed more selectively, and information may be sorted out with more confidence. More examples of application of the SSSE to complex redox systems have been described elsewhere.[28]

References

1. T. Kuwana and N. Winograd in "*Electroanalytical Chemistry*", A. J. Bard, ed., Marcel Dekker, New York, Vol. 1, p.1. 1974.
2. R. H. Müller, ed., "*Advances in Electrochemistry and Electrochemical Engineering*", Wiley-Interscience, New York, Vol. 8 1973.
3. T. Kuwana and W. R. Heineman, *Acc. Chem. Res.*, **9**, 241 (1976).
4. R. Miles, *Surf. Interface Anal.*, **5**, 43 (1983).
5. J. Robinson in "*Electrochemistry-Specialist Periodical Reports*", D. Pletcher, ed., The Royal Society of Chemistry, Burlington House, London, Vol. 9 1984.
6. E. E. Bancroft, J. S. Sidwell, and H. N. Blount, *Anal. Chem.*, **53**, 1390 (1981).
7. E. E. Bancroft, H. N. Blount, and F. M. Hawkridge in "*Electrochemical and Spectrochemical Studies of Biological Redox Components*", K. M. Kadish, ed., Advances in Chemistry, Series 201, American Chemical Society, Washington, DC, 1982.
8. C.-H. Pyun and S.-M. Park, *Anal. Chem.*, **58**, 251 (1986).
9. J. P. Skully and R. L. McCreery, *Anal. Chem.*, **52**, 1885 (1980).
10. C.-H. Pyun and S.-M. Park, *J. Electrochem. Soc.*, **132**, 2426 (1985).
11. C.-H. Pyun and S.-M. Park, *J. Electrochem. Soc.*, **133**, 2024 (1986).
12. C. Zhang and S.-M. Park, *J. Electrochem. Soc.*, **134**, 2966 (1987).
13. D. E. Stilwell and S.-M. Park, *J. Electrochem. Soc.*, **136**, 427 (1989).
14. C. Zhang and S.-M. Park, *Anal. Chem.*, **60**, 1639 (1988).
15. A. J. Bard and L. R. Faulkner, "*Electrochemical Methods*", John Wiley & Sons, New York, 1980.
16. D. E. Albertson, H. N. Blount, and F. M. Hawkridge, *Anal. Chem.*, **51**, 556 (1979).
17. F. C. Anson, *Anal. Chem.*, **38**, 54 (1966).
18. C. L. Bird and A. T. Kuhn, *Chem. Soc. Rev.*, London, **10**, 49 (1981).
19. M. Ito and T. Kuwana, *J. Electronal. Chem.*, **32**, 425 (1971).
20. N. Winograd and T. Kuwana, *J. Am. Chem. Soc.*, **92**, 224 (1970).
21. E. Steckhan and T. Kuwana, *Ber. Bunsenges. Phys. Chem.*, **78**, 253 (1974).
22. E. M. Kosower and J. L. Lotter, *J. Am. Chem. Soc.*, **86**, 5524 (1964).
23. W. M. Schwarz, Jr., Ph.D. Dissertation, University of Wisconsin, 1961.
24. J. Bruinink, C. G. A. Kregting, J. J. Ponje, *J. Electrochem. Soc.*, **124**, 1854 (1977).
25. D. G. Peters and S. L. Burden, *Anal. Chem.*, **38**, 530 (1966).
26. P. E. Sturrock, J. L. Hughey, B. Vaudreuil, G. O'Brien, and R. H. Gibson, *J. Electrochem. Soc.*, **122**, 1195 (1975).
27. P. E. Sturrock and R. H. Gibson, *J. Electrochem. Soc.*, **123**, 629 (1976).
28. C. Zhang and S.-M. Park, *J. Electrochem. Soc.*, **136**, in press (1989).